Journal of Medicinal Chemistry

Article

pubs.acs.org/jmc

Structure-Based Optimization of Tyrosine Kinase Inhibitor CLM3. Design, Synthesis, Functional Evaluation, and Molecular Modeling Studies.

Stefania Sartini,[†] Vito Coviello,[†] Agostino Bruno,[‡] Valeria La Pietra,[‡] Luciana Marinelli,[‡] Francesca Simorini,[†] Sabrina Taliani,[†] Silvia Salerno,[†] Anna Maria Marini,[†] Anna Fioravanti,[§] Paola Orlandi,[§] Alessandro Antonelli,[§] Federico Da Settimo,[†] Ettore Novellino,[‡] Guido Bocci,[§,∥] and Concettina La Motta*[,†]

[†]Dipartimento di Farmacia, Università di Pisa, Via Bonanno 6, 56126 Pisa, Italy

[‡]Dipartimento di Farmacia, Università di Napoli "Federico II", Via D. Montesano, 49, 80131 Napoli, Italy

[§]Dipartimento di Medicina Clinica e Sperimentale, Università di Pisa, Via Roma 55, 56126 Pisa, Italy

[∥]Istituto Toscano Tumori, Via T. Alderotti 26N, 50139 Firenze, Italy

Supporting Information

ABSTRACT: Recent advances in the knowledge of thyroid carcinomas development identified receptor tyrosine kinases, like VEGFR2 and RET, as viable and promising targets. Accordingly, their inhibition is emerging as the major therapeutic strategy to treat these pathologies. In this study we describe the synthesis and the functional evaluation of three different series of 4-substituted pyrazolo[3,4-*d*]pyrimidine derivatives, **8a**−**g**, **9a**−**g**, and **10a**−**g**, designed exploiting a structure-based optimization of the previously developed inhibitor **CLM3**. Compared to the lead, the novel compounds markedly improved both their inhibitory profile against the target proteins, VEGFR2 and RET, and their antiproliferative efficacy against the medullary thyroid cancer cell line TT. Significantly, compounds **8b**, **9c**, and **10c** proved to block the kinase activity of the mutant RET^{V804L}, which still lacks effective inhibitors.

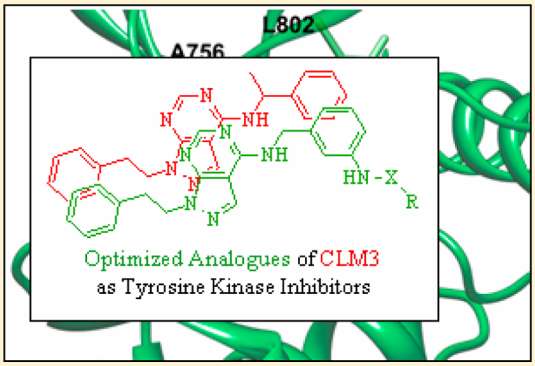

INTRODUCTION

Thyroid carcinomas (TCs) are the most common endocrine tumors, accounting for up to 1% of all human malignancies. Their worldwide incidence rate has been increasing sharply since the mid-1990s, thus becoming the fastest increasing type of cancer in both men and women in Western countries. According to American Cancer Society forecasts, in 2013 there will be about 60 000 novel cases of TCs diagnosed in U.S., with three to four cases occurring in women, and almost 2000 deaths due to TCs in both sexes, thus indicating a marked acceleration in the incidence rate of the past decade of 5.5% and 6.6% per year in men and women, respectively.[1−3]

To date, the treatment of choice for different forms of TCs relies in their complete surgical resection, possibly associated with external radiation therapy. However, disease can persist or recur with local and distant metastases, and in these cases, outcomes are poor, with 5-year survival rates lower than 50%, often associated with a marked resistance to cytotoxic chemotherapy.

Indeed, endocrine cancers are generally resistance to DNA-damaging chemotherapies or radiotherapy, normally exploited to lead cancer cells to apoptosis.[4,5] Accordingly, novel therapeutic strategies are urgently needed. Recent advances in the knowledge of pathogenic mechanisms leading to TCs clearly demonstrate that oncogenic tyrosine kinases sustain their development and/or progression, thus identifying these proteins as new and promising targets. "Gain of function" mutations and/or rearrangement of tyrosine kinase receptors like EGFR and RET, as well as signaling molecules acting downstream through BRAF, RAS/RAF/ERK, and RAS/PI3K/AKT pathways, can trigger cell transformations in TCs, thus providing mitogenic and survival signals. Mutations of the tyrosine kinase receptor RET have been identified in about 98% of inherited medullary thyroid carcinoma (MTC) cases at the germ-line level and in 30−50% of the sporadic cases at the somatic level. RET rearrangement is also the most common genetic abnormality in papillary thyroid carcinoma (PTC) induced by radiation. EGFR and its ligands are implicated in TCs, having been found in all types of TCs. Moreover, TCs often exhibit markedly increased vascularisation and elevated VEGF expression. Indeed, VEGF receptors have been found on TC cell lines and tumor endothelial cells, and increased VEGF levels have been determined in the serum/plasma of thyroid

Received: August 2, 2013
Published: January 21, 2014

   dx.doi.org/10.1021/jm401358b | *J. Med. Chem.* 2014, 57, 1225−1235

Chart 1. Tyrosine Kinase Inhibitors

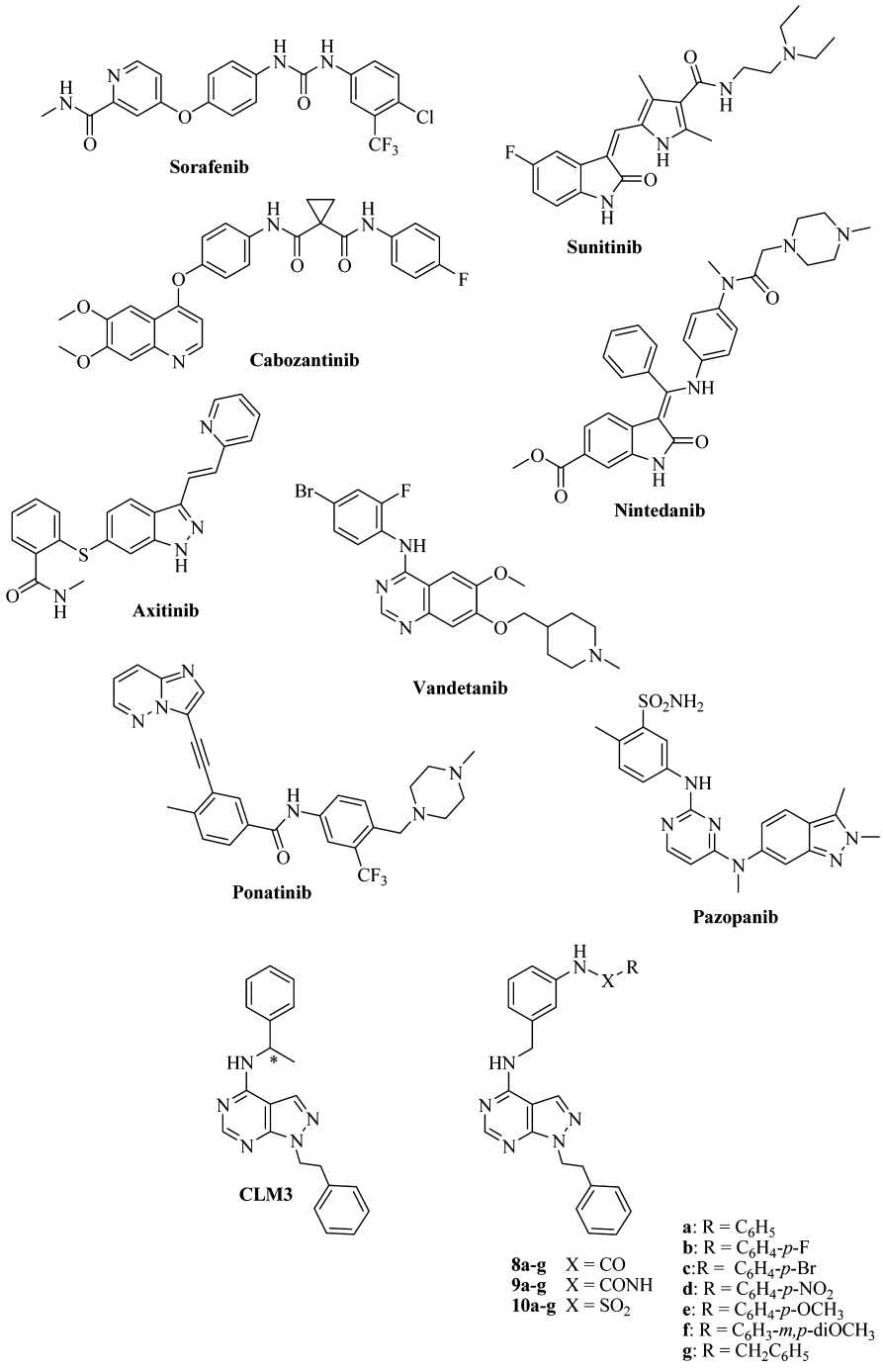

cancer patients. These outcomes correlate positively with high tumorigenic potential, thus clearly highlighting angiogenesis as an important factor in tumor growth and metastasis. Protein kinases therefore represent a sound target for the molecular therapy of people affected by TCs, and their inhibition is now accepted as an effective therapeutic strategy.[6−12]

Different approaches have been considered to block the kinase activity of the mentioned proteins, the most pursued one being the use of small molecules able to compete with the ATP site of their catalytic domain. These include compounds already approved throughout the world for the treatment of other types of tumors, like sorafenib[13] and sunitinib[14] (Chart 1), and novel derivatives such as ponatinib,[15] nintedanib,[16] axitinib,[17] and pazopanib[18] (Chart 1), either proposed or already enrolled in phases II and III clinical trials for TCs. However, to date, the only commercially available tyrosine kinase inhibitors approved by FDA for the treatment of symptomatic or progressive advanced and metastatic MTC are the quinazolin-4-amino derivative vandetanib[19] and the quinoline derivative cabozantinib[20] (Chart 1). Similar to the previously mentioned derivatives, they both are multitarget compounds, being able to combine a potent antiangiogenic activity, mainly due to VEGFR2 inhibition, with inhibitory properties against additional protein kinases. Accordingly, affecting simultaneously different mitogenic pathway in both cancer cells and vasculature, they are able to control both tumor growth and

dx.doi.org/10.1021/jm401358b | J. Med. Chem. 2014, 57, 1225−1235

Scheme 1. Synthesis of Pyrazolo[3,4-*d*]pyrimidine Derivatives 8a−g, 9a−g, and 10a−g

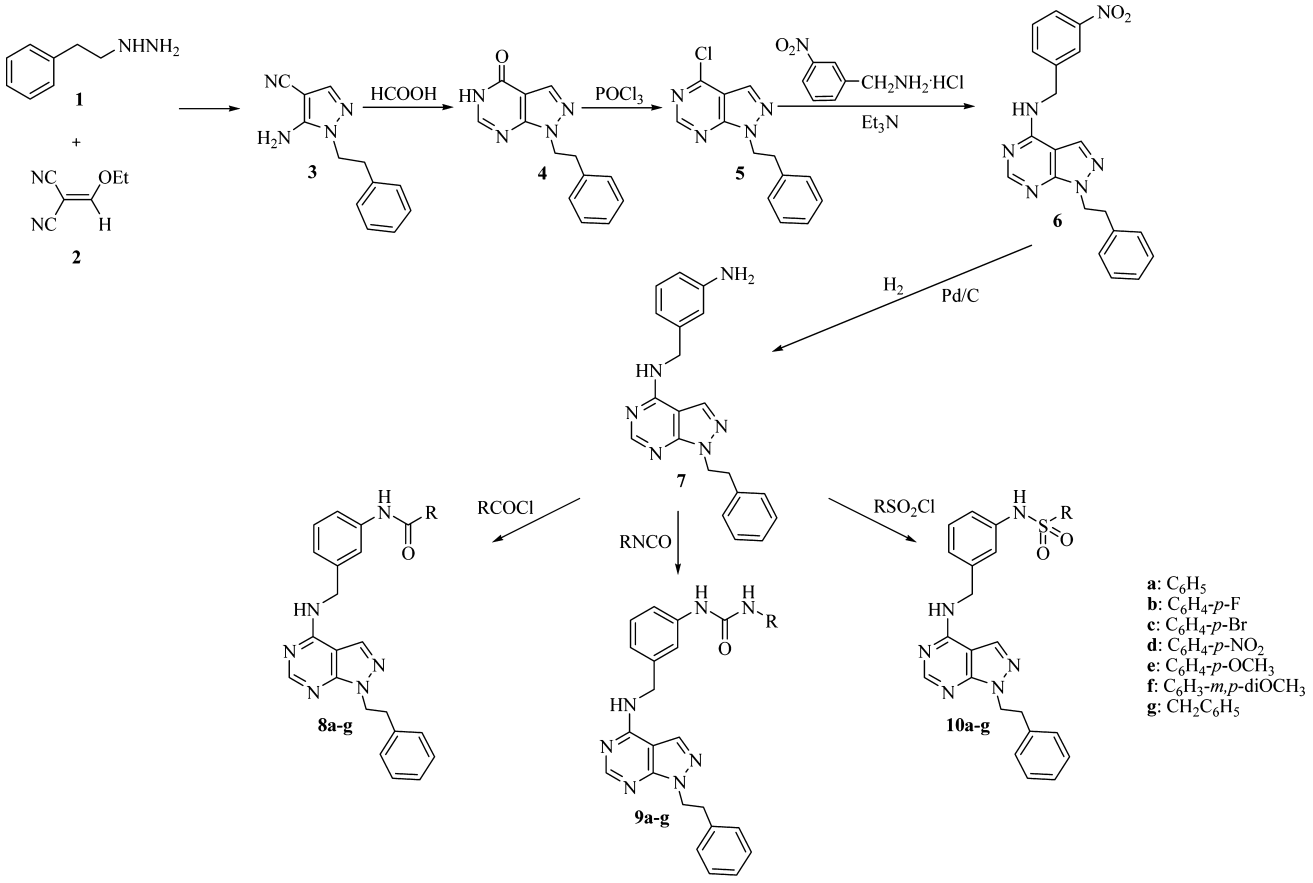

metastasis. However, their significant efficacy is often associated with serious toxicities, including osteonecrosis, fatal hemorrhages, hypertension, QTc prolongation, and respiratory failures.[21] Moreover, as regard to vandetanib, acquired resistance has been indicated, mainly driven by point mutations of the target proteins, which strongly limits its exploitation as a plain and widespread therapeutic agent against TCs.[22] Accordingly, the search of novel tyrosine kinase inhibitors is highly welcome, as novel clinically effective and safe compounds to treat TCs are strongly required.

Our research group has been involved in the development of novel tyrosine kinase inhibitors for many years, to achieve novel drug candidates for the treatment of TCs. Focusing on the pyrazolo[3,4-*d*]pyrimidine heterocyclic core, a privileged scaffold in the tyrosine kinase inhibitors field,[23−26] we recently disclosed a new derivative, (*R*)-1-phenethyl-*N*-(1-phenylethyl)-1*H*-pyrazolo[3,4-*d*]pyrimidin-4-amine, namely, **CLM3** (Chart 1), which proved to combine an excellent antiangiogenic efficacy with a less marked inhibitory activity against human thyroid cancer cell lines, both demonstrated through time- and concentration-dependent antiproliferative and proapoptotic activities on specific cell lines.[27,28] Actually, the microvascular endothelial cell line HMVEC-d was remarkably sensitive to low concentrations of **CLM3** (IC_{50} = 0.40 ± 0.22 nM after 72 h of exposure), whereas thyroid cancer cell lines as the undifferentiated 8305C (IC_{50} = 9.20 ± 5.06 μM after 72 h of exposure), expressing endogenous RET, and the medullary TT (IC_{50} = 26.93 ± 7.60 μM), expressing the mutated protein, required higher concentrations to be inhibited in their growth. Tested on papillary dedifferentiated thyroid cancer cell line (DePTC), obtained at reoperation from patients with recurrence of the tumor, **CLM3** proved to inhibit significantly its proliferation, increasing the percentage of apoptotic cells and inhibiting their migration in a dose-dependent manner. Moreover, when administered to CD nu/nu mice xenotransplanted with the same DePTC cell line, CLM3 proved to inhibit both tumor growth and weight, without showing any appreciable toxicity.[27]

Taken together, these results were extremely encouraging, as they affirmed **CLM3** as a sound and viable lead candidate, deserving of further development. Accordingly, guided by preliminary docking studies performed on the target kinases, we embarked in rational optimization of **CLM3**, with the purpose of obtaining novel and effective dual VEGFR2/RET inhibitors.

In this work we present the synthesis of new derivatives of **CLM3**, whose benzylamino substituent at position 4 of the heterocyclic core was suitably lengthened through the insertion of arylamido (**8a−g**, Chart 1), arylureido (**9a−g**, Chart 1), and arylsulfonyl (**10a−g**, Chart 1) groups. These were chosen to plainly comply with pharmacophore requirements of the ATP binding sites of both VEGFR2 and RET, highlighted by the aforementioned docking studies. All of the synthesized compounds were evaluated for their inhibitory properties against the target tyrosine kinases and for their antiproliferative activity toward both endothelial and human thyroid cancer cell lines.

CHEMISTRY

The target inhibitors **8a−g**, **9a−g**, and **10a−g** were synthesized as illustrated in Scheme 1. Reaction of phenethylhydrazine, **1**,[29] with the commercially available 2-(ethoxymethylene)-

dx.doi.org/10.1021/jm401358b | J. Med. Chem. 2014, 57, 1225−1235

malononitrile, **2**, gave the pyrazole derivative, **3**, whose cyclization with boiling formic acid provided the 1-phenethyl-1*H*-pyrazolo[3,4-*d*]pyrimidin-4(5*H*)-one, **4**. Treatment of **4** with phosphoryl trichloride in DMF afforded the corresponding 4-chloro derivative, **5**, which led to the intermediate **6** by reaction with (3-nitrophenyl)methanamine, in the presence of triethylamine. Catalytic hydrogenation of **6** carried out with 10% Pd on carbon at room temperature and atmospheric pressure gave the key amino derivative **7**, which was then treated with the suitable reactants to give the target inhibitors. In particular, reaction with the appropriate aroyl chloride in the presence of triethylamine led to compounds **8a–g**, treatment with the suitable isocyanate provided the urea derivatives **9a–g**, and addition of substituted sulfonyl chlorides afforded the sulfonamido inhibitors **10a–g**.

RESULTS AND DISCUSSION

Structure-Based Lead Optimization. We started our optimization campaign testing **CLM3** in vitro on the human recombinant target proteins, VEGFR2 and RET, to confirm its ability to compete with the ATP site of the tyrosine kinases. When an IC_{50} value of 52.5 μM against VEGFR2 was obtained and the ability of **CLM3** to halve the kinase activity of RET was verified (Table 1), we then clarified its mode of binding to both of the target proteins, exploiting preliminary docking calculations. In the case of VEGFR2, Glide software[30] positioned **CLM3** into the X-ray structure of the protein (PDB code 4AG8[31]) so that the N2 of the pyrazolopyrimidine ring can establish an H-bond with the C919 backbone, the phenylethanamine moiety is surrounded by V848, K868, A866, L889, L1035, and V916 side chains, while the phenylethyl group forms hydrophobic contact with L840 and F918 residues. As highlighted in Figure 1, the short substitution pattern on position 4 of the heterocyclic core prevents **CLM3** from reaching the VEGFR2 regulatory domain pocket (RDP), represented by the cleft enclosed by the juxtamembrane domain of the receptor refolding into the catalytic site. Accordingly, interactions with key E885 and D1046 residues, often hooked by known VEGFR2 inhibitors from the literature, like sorafenib,[31] are precluded, and this observation can be instrumental to improve **CLM3** binding toward VEGFR2.

At the same time, docking of **CLM3** in the ATP domain of RET kinase (PDB code 2IVV[32]) resulted in the binding mode shown in Figure 2. Specifically, in the lowest-energy binding pose, the N5 atom of the pyrazolopyrimidine ring establishes an H-bond with the A807 backbone, **CLM3** central core is stacked between A756, V738, and L881, while the phenylethyl moiety occupies the N-lobe, thus establishing hydrophobic interactions with V804, L802, I788, L779, and K758 side chains. The phenylethanamine moiety is pretty solvent exposed, and this position could reasonably account for the lower activity of **CLM3** toward RET, deduced through functional evaluation on 8305C and TT cell lines, expressing the target receptor kinase, and on the human recombinant protein.

Thus, binding modes obtained for **CLM3** in both VEGFR and RET sites clearly suggested the structural limitations of **CLM3**, but at same time, they pave the way for a **CLM3** rational modification. Actually, on the bases of the docking results obtained with VEGFR2, we decided to functionalize the meta position of the phenylethanamine ring with a number of substituents able to fill the RDP of the protein. Accordingly, differently para-substituted phenyl rings bridged with amide, urea, or sulfonamide moieties, already exploited for the obtainment of VEGFR2 inhibitors from the literature,[23,33,34] were inserted on the ring. At same time, to confer major flexibility to this substituent, thus allowing an easier accommodation inside the RDP, the methyl group of the phenylethanamine function was removed. On the basis of the suggested **CLM3** binding mode in the RET active site, the

Table 1. Tyrosine Kinases Inhibitory activity of Derivatives 8a–g, 9a–g, and 10a–g

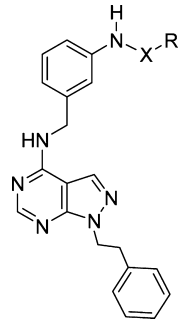

			IC_{50},[a] μM	
compd	X	R	VEGFR2	RET
8a	CO	C_6H_5	8.57	22.4
8b	CO	C_6H_4-4-Br	3.48	4.26
8c	CO	C_6H_4-4-F	5.37	9.64
8d	CO	C_6H_4-4-NO_2	3.29	17.1
8e	CO	C_6H_4-4-OCH_3	2.66	24.1
8f	CO	C_6H_3-3,4-diOCH_3	2.03	28.1
8g	CO	$CH_2C_6H_5$	6.45	22.6
9a	CONH	C_6H_5	2.16	7.04
9b	CONH	C_6H_4-4-Br	3.40	9.07
9c	CONH	C_6H_4-4-F	3.17	4.80
9d	CONH	C_6H_4-4-NO_2	1.09	37[b]
9e	CONH	C_6H_4-4-OCH_3	1.09	9.26
9f	CONH	C_6H_3-3,4-diOCH_3	3.27	15.3
9g	CONH	$CH_2C_6H_5$	6.74	10.3
10a	SO_2	C_6H_5	4.96	7.90
10b	SO_2	C_6H_4-4-Br	4.89	12.85
10c	SO_2	C_6H_4-4-F	2.89	4.83
10d	SO_2	C_6H_4-4-NO_2	1.03	57[b]
10e	SO_2	C_6H_4-4-OCH_3	3.87	57.2
10f	SO_2	C_6H_3-3,4-diOCH_3	7.21	8[b]
10g	SO_2	$CH_2C_6H_5$	2.23	58.6
CLM3			52.5	48[b]

[a]IC_{50} values represent the concentration required to produce 50% enzyme inhibition. Standard error of the mean (SEM) is ≤10%. [b]Percentage of kinase inhibition at 100 μM test compound.

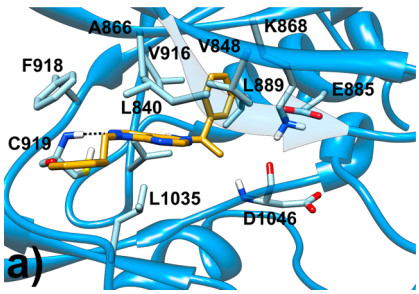

Figure 1. Putative binding pose of **CLM3** (gold sticks) in the active site of VEGFR-2 shown as blue cartoon and cyan sticks. H-bonds are represented as black dashed lines and part of the backbone is in transparent ribbon, for clarity reason.

dx.doi.org/10.1021/jm401358b | J. Med. Chem. 2014, 57, 1225–1235

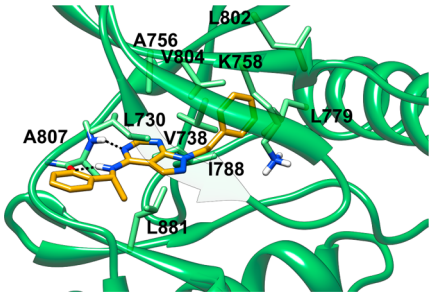

Figure 2. Putative binding pose of **CLM3** (gold sticks) in the active site of RET kinase shown as green cartoons. H-bonds are represented as black dashed lines and part of the backbone is in transparent ribbon, for clarity reason.

introduction of polar substituents on the phenylethanamine group was expected to be beneficial.

Synthesis and Functional Evaluation of Novel Pyrazolo[3,4-*d*]pyrimidines. Guided by the preliminary docking studies, we started our structural optimization synthesizing compounds **8a**−**g**, characterized by the presence of a benzamide residue in the meta position of the N^4-benzyl group of **CLM3**. As reported in Table 1, listing functional activities expressed as IC_{50} values, all the novel compounds showed a remarkable enhancement in inhibitory efficacy against the target proteins when compared to the starting lead. In the case of VEGFR2, compound **8a** (IC_{50} = 8.57 μM) displayed a 6-fold increase in inhibitory potency with respect to **CLM3** (IC_{50} = 52.5 μM). The insertion of electron-withdrawing substituents in the para position of the distal phenyl ring, as in **8b** (IC_{50} = 3.48 μM), **8c** (IC_{50} = 5.37 μM), and **8d** (IC_{50} = 3.29 μM), enhanced the observed activity, but an even better raise in inhibitory potency was obtained through the insertion of electron-donating groups. Indeed, the presence of a methoxy function, as in **8e** (IC_{50} = 2.66 μM), gave a 20-fold gain in inhibitory activity with respect to **CLM3**, and compound **8f**, bearing a dimethoxy substituent pattern, turned out to be the best VEGFR2 inhibitor of the whole subseries, showing an IC_{50} value of 2.03 μM. Finally, an increase in the distance between the phenyl ring and the amide linker through a methylene spacer was well tolerated, with **8g** (IC_{50} = 6.45 μM) being almost equipotent to the unsubstituted parent **8a**. As regard to RET, a significant inhibitory efficacy was observed as well. Moving from **8a** (IC_{50} = 22.4 μM), the insertion of electron-donating groups like methoxy (**8e**, IC_{50} = 24.1 μM) and dimethoxy (**8f**, IC_{50} = 28.1 μM) did not affect the activity, and the same was also true for the lengthened derivative **8g** (IC_{50} = 22.6 μM). On the contrary, the presence of electron-withdrawing groups as in **8b** (IC_{50} = 4.26 μM), **8c** (IC_{50} = 9.64 μM), and **8d** (IC_{50} = 17.1 μM) gave a 1.5- to 5-fold increase of efficacy. Significantly, the presence of a bromine atom in the para position of the distal ring guaranteed the highest inhibitory activity against the target protein, with **8b** being the best dual inhibitor of the whole subseries.

Analogous results were obtained through the synthesis of derivatives **9a**−**g**, where the N^4-benzyl group of the lead, **CLM3**, was functionalized with a phenylureido moiety. Concerning VEGFR2, all the compounds displayed a remarkable activity. Actually, with respect to the lead, the unsubstituted **9a** (IC_{50} = 2.16 μM) showed an almost 25-fold gain in efficacy. The different substituents in the para position of its distal ring, independent of their electronic nature, keep unaltered this excellent inhibitory property, as the resulting compounds **9b**−**f** showed IC_{50} values ranging from 1.09 to 3.40 μM. The lengthened **9g** (IC_{50} = 6.74 μM) was active as well. As regards RET, the significant activity of the unsubstitued **9a** (IC_{50} = 7.04 μM) was gradually reduced by the presence of a bromine atom, as in **9b** (IC_{50} = 9.07 μM), a methoxy (**9e**, IC_{50} = 9.26 μM), and a dimethoxy group (IC_{50} = 15.3 μM). The observed trend reached the peak with **9d**, bearing a nitro group, which reduced slightly the kinase activity of the target protein. On the contrary, the lengthened derivative **9g** proved to be almost equipotent to the unsubstituted parent compound **9a**. Also in this subseries, the presence of an halogen atom turned out to be the best substitution pattern to obtain a potent dual inhibitor, as compound **9c**, bearing a para fluorine atom (VEGFR2, IC_{50} = 3.17 μM, RET, IC_{50} = 4.80 μM), displayed the best inhibitory profile.

The choice to modify the lead, **CLM3**, exploiting a benzenesulfonamide group, as in **10a**−**g**, led to potent VEGFR2 inhibitors. Moving from the unsubstituted **10a** (IC_{50} = 4.96 μM) the insertion of either a bromine atom, as in **10b** (IC_{50} = 4.89 μM), or methoxy groups, as in **10e** (IC_{50} = 3.87 μM) and **10f** (IC_{50} = 7.21 μM), did not modify significantly the inhibitory activity, while the selective presence of a nitro group (**10d**, IC_{50} = 1.03 μM), as well as the insertion of a methylene spacer (**10g**, IC_{50} = 2.23 μM) exerted a positive effect on the observed efficacy. On the contrary, with respect to the tyrosine kinase RET, the benzenesulfonamide moiety gave rise to contrasting results. Actually, for the unsubstituted **10a** (IC_{50} = 7.90 μM), the presence of either a bromine atom (**10b**, IC_{50} = 12.8 μM) or a nitro function (**10d**, 57% inhibition at 100 μM), a methoxy (**10e**, IC_{50} = 57.2 μM), and a dimethoxy group (**10f**, 8% inhibition at 100 μM) gave rise to a progressive loss of activity. The same was also true for the lengthened derivative **10g**, showing an IC_{50} value of 58.6 μM. On the contrary, the insertion of a fluorine atom restored a remarkable inhibitory efficacy. Indeed, once again, also in this subseries, the presence of this kind of substituent led to the best dual inhibitory pattern, and compound **10c**, with IC_{50} values of 2.89 and 4.83 μM against VEGFR2 and RET, respectively, turned out to be the most effective one of all the benzenesulfonamide derivatives.

The best performing derivatives, **8b**, **9c**, and **10c**, were also assayed on the mutant human recombinant RET^{V804L}, occurring in both spontaneous and familial MTC, which proved to be insensitive to the already known kinase inhibitors, including the commercially approved vandetanib. Significantly, all the test compounds were demonstrated to block the kinase activity of the mutant protein, showing IC_{50} values ranging from 5.47 to 9.31 μM (Table 2).

Functional Evaluation on HUVEC, TT, and HNDF Cell Lines. Representative examples of the three subseries **8a**−**d**, **9a**,**b**, and **10a**,**g** were tested on HUVEC and TT cells to explore

Table 2. RET^{V804L} Inhibitory Data of Derivatives 8b, 9c, and 10c

compd	RET^{V804L} IC_{50},[a] μM
8b	9.31
9c	7.96
10c	5.47

[a]IC_{50} values represent the concentration required to produce 50% enzyme inhibition. Standard error of the mean (SEM) is ≤10%.

dx.doi.org/10.1021/jm401358b | *J. Med. Chem.* 2014, 57, 1225−1235

their ability to inhibit proliferation of these selected lines. After a 72-h exposure, all the test derivatives proved to block cells growth in a concentration dependent manner (Table 3).

Table 3. Inhibitory Activity of Derivatives 8a–d, 9a,b, and 10a,g against HUVEC and TT Cell Lines

	IC_{50},[a] μM	
compd	HUVEC	TT
8a	15.31 ± 0.59	13.82 ± 1.32
8b	9.83 ± 0.97	13.48 ± 2.30
8c	15.93 ± 1.31	13.57 ± 3.88
8d	16.64 ± 0.88	6.13 ± 1.74
9a	13.43 ± 4.55	8.42 ± 1.26
9b	18.55 ± 0.007	9.86 ± 0.72
10a	22.64 ± 1.13	8.08 ± 1.10
10g	50.73 ± 9.25	5.97 ± 1.17

[a]IC_{50} ± SD values represent the concentration of drug that decreased cell count by 50%.

Significantly, when compared to **CLM3**, the novel compounds determined a greater and very promising activity on TT cell proliferation, showing IC_{50} values in the low micromolar range and a 5-fold gain of efficacy with respect to the parent lead. The functional efficacy observed on TT cell lines was further investigated by evaluating the ability of the most active derivatives, namely, **8d**, **9a**, and **10a**,**g**, to inhibit the phosphorylation of the target receptor. After exposure to the test compounds, the ratio of phosphorylated/nonphosphorylated RET protein of treated cells was significantly decreased in TT cell lines (Table 4), thus confirming that the antiproliferative activity of the compounds is mainly due to their inhibition of phosphorylation of RET.

Table 4. Inhibitory Activity of RET Phosphorilation of Derivatives 8d, 9a, 10a, and 10g[a]

compd	% of (pRET)/(total RET) vs 100% of control
8d	66.4 ± 4.9*
9a	64.5 ± 12.6*
10a	88.7 ± 4.4
10g	68.9 ± 1.7*

[a]Results were obtained from experiments using compounds at their respective antiproliferative IC_{50} values: mean ± SD, (*) $P < 0.05$ vs control.

Finally, compounds **8d** and **10g** were also tested on cycling normal human fibroblast HNDF line to investigate their antiproliferative activity on a noncancerous cell line. Test compounds showed IC_{50} values of 22.0 ± 2.0 μM (mean ± SD) and 23.6 ± 1.2 μM (mean ± SD), respectively. These IC_{50} values were almost 4-fold higher than the ones observed in the TT tumor cell line, thus confirming the preferential activity of the compounds on the cell line with mutated RET.

Structure–Activity Relationships and Docking Studies. All the compounds reported in Table 1 were docked in the VEGFR2 active site. Here, we have shown and analyzed in detail the binding mode of compound **10c** (Figure 3a) as the main representative of the three new series of VEGFR2 inhibitors. Binding modes obtained for **CLM3** (Figure 1) and **10c** (Figure 3a) in VEGFR2 were highly superimposable. The main differences reside in further interactions with E885 and D1046, established by the sulfonamide group of **10c** (Figure 3a), and with L889, I892, V899, L1019, H1026 (RDP), engaged with the pendent phenyl ring, which accounts for the 11-fold increase in inhibitory potency observed for **10c** when compared to **CLM3**. Notably, all the novel derivatives, regardless their polar bridge groups, CO, CONH, and SO_2, showed highly similar pattern of interactions as described for **10c** (see Figure 1-SI in Supporting Information), thus legitimating the gain in inhibitory potency of all the novel derivatives with respect to **CLM3**. Specifically, in the **8a–g** subseries, the short bridge did not allow a complete fill of the RDP. Indeed, compounds **8a** was less active than **9a** and **10a**, but the introduction of 4-substituents on the distant phenyl ring further improved the inhibitory potency. Regarding the RET kinase, binding modes obtained for the most active compounds of the amide and urea series, **8b** and **9c**, respectively (Figure 4), were pretty superimposable with that of **CLM3** (Figure 2), with main differences residing in further possible interactions of amide and urea linkers and the terminal phenyl ring lodged near the region of where the AMP phosphate group binds (PDB code 2IVT,[32] Figure 4a). Indeed, both linkers are in proximity to S811 and an H-bond is likely to occur. Meanwhile the 4-substituted benzene ring is just above the N879 amidic side chain, thus justifying a general improvement in the IC_{50} values toward RET. Furthermore, the substitution of the aforementioned benzene with a bromine atom, in the case of the shorter amide linker (**8b**), and with a fluorine atom, in the case of the longer urea bridge (**9c**), gave the possibility of establishing an H-bond with the NH group of the E734, thus producing lower IC_{50} values with respect to their nonhalogenated counterparts (Figure 4a and Figure 4b). Finally, docking of **10c** (Figure 3b) shown that the sulfonamide moiety establishes multiple H-bonds with the hydroxyl and ammonium groups of the Y806, K728, and K740 side chains, respectively. However, the peculiar geometry of the sulfonamide group forces the phenyl ring to occupy a different portion,

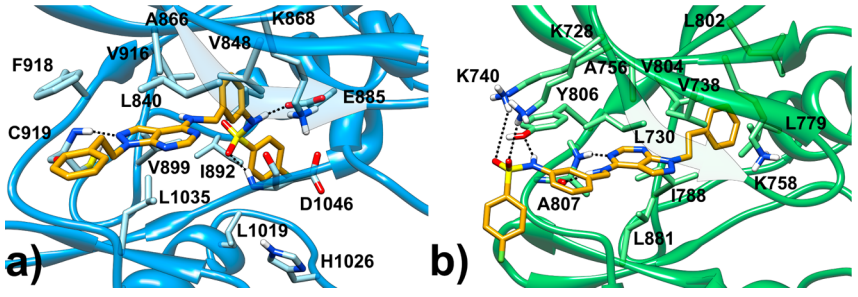

Figure 3. Binding pose of **10c** (gold sticks) in the active site of VEGFR-2 (a) and RET (b) shown as blue and green cartoons, respectively. H-bonds are shown as black dashed lines and part of the backbone is in transparent ribbon, for clarity reason.

dx.doi.org/10.1021/jm401358b | J. Med. Chem. 2014, 57, 1225–1235

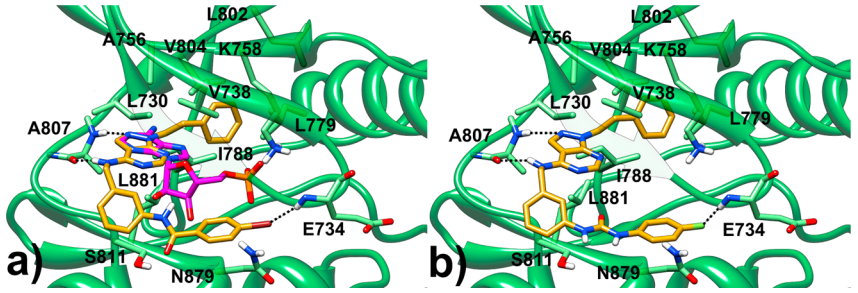

Figure 4. Binding pose of **8b** (a) and **9c** (b) represented as gold sticks in the active site of RET, shown as green cartoon. H-bonds are shown as black dashed lines and part of the backbone is in transparent ribbon, for clarity reason. Cocrystallyzed AMP molecule is superimposed with **8b** (a).

where it is partially solvent exposed, thus accounting for the lower activity of **10e−10g**, while a general improved activity is observed for the halogenated compounds, as for **10c**.

Finally, with the aim to gain information about the capability of **8b**, **9c**, and **10c** to bind RET^{V804L}, docking was performed using the mutated RET as the target receptor, showing that the flexible phenylethyl moiety is able to shift its position with respect to that observed when calculations are performed on RET wild type. Particularly, when the three compounds are docked in RET^{V804L}, the phenylethyl branch rearranges itself and occupies the region where AMP phosphate group binds, thus losing interactions with L779 and L802 side chains and, at the same time, gaining hydrophobic contacts with V738 and L881 side chains. Obviously, while for **10c** (Figure 5a) the

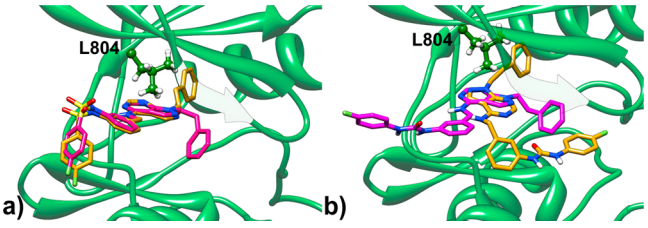

Figure 5. Superposition of the docking binding poses of **10c** (a) and **9c** (b) into the WT (golden sticks) and V804L mutant (magenta sticks) RET kinase. The active site of RET is shown as green cartoon although part of the backbone is in transparent ribbon, for clarity reason. The L804 residue is represented as balls and sticks.

novel position of the phenylethyl moiety does not affect the rest of the binding mode, in the case of **8b** and **9c**, the amide and ureidic linkers with the distant phenyl ring have to readjust altogether, and as shown in Figure 5b, these branches come to occupy the same region of the sulfonamide moiety of **10c**.

CONCLUDING REMARKS

In this work we presented a successful example of structure-based optimization, pursued on the known tyrosine kinase inhibitor **CLM3**.[27,28] Guided by preliminary docking studies, we rationally explored different substitution patterns on the heterocyclic core, with the purpose of improving the dual inhibitory profile of the starting lead.

The novel synthesized compounds displayed a remarkable increase in inhibitory potency against the target proteins, showing IC_{50} values in the micromolar range. Significantly, the best performing ones, **8b**, **9c**, and **10c**, proved to inhibit also the mutant RET^{V804L} which, to date, is the main cause of functional failure of the well-known tyrosine kinase inhibitors from the literature, including the commercially approved vandetanib which is devoid of any inhibitory efficacy against this form of protein.

A preliminary evaluation on both endothelial and medullary thyroid cancer cell lines revealed the promising antiproliferative profile of the novel derivatives. Compared to the lead, **CLM3**, the test compounds exhibited a remarkable increase in efficacy against the target thyroid cancer cell line TT, expressing mutated RET, showing an almost 5-fold decrease of IC_{50} values, as in **8d** (6.13 ± 1.74 μM) and **10g** (5.97 ± 1.17 μM). Despite a concurrent inflection in the antiproliferative activity against the HUVEC cell lines, the novel compounds possess a better balanced dual target profile, thus improving, in principle, their therapeutic efficacy against the complex network of proteins accountable for both the pathogenesis and progression of TCs.

Interestingly, the functional efficacy observed for the novel compounds here described is fully comparable to the ones shown by the already commercially approved tyrosine kinase inhibitors cabozantinib and vandetanib, tested by Verbeek and co-workers[35] in analogous assays conditions.

Further studies in animal models will prove their robustness as prototypical drug candidates exploitable for the treatment of TCs, including the medullary thyroid cancer, which is caused by RET activating mutations and still needs a viable and effective therapeutic solution.

EXPERIMENTAL SECTION

Chemistry. Melting points were determined using a Reichert Köfler hot-stage apparatus and are uncorrected. Routine ^{1}H NMR spectra were recorded in DMSO-d_6 solution on a Varian Gemini 200 spectrometer operating at 200 MHz. Mass spectra were obtained on a Hewlett-Packard 5988 A spectrometer using a direct injection probe and an electron beam energy of 70 eV. Evaporation was performed in vacuo (rotary evaporator). Analytical TLC was carried out on Merck 0.2 mm precoated silica gel aluminum sheets (60 F-254). Microwave-assisted reactions were carried out in sealed vessels using a Biotage initiator 2.5 microwave synthesizer. Purity of the target inhibitors, **8a−g**, **9a−g**, and **10a−g**, was determined by HPLC analysis, using a Merck Hitachi D-7000 liquid chromatograph (UV detection at 242 nm) and a Discovery C18 column (250 mm × 4.6 mm, 5 μm, Supelco), with a gradient of 30% water and 70% methanol and a flow rate of 1.5 mL/min. All the compounds showed percent purity values of ≥95% (Table 7-SI, Supporting Information).

2-(Ethoxymethylene)malononitrile, 3-nitrobenzylamine hydrochloride, and the suitably substituted aroyl chlorides, arylsulfonyl chlorides, and aryl isocyanates, used to obtain the target inhibitors, were from Alfa Aesar, Aldrich, and Fluka.

Synthesis of 5-Amino-1-phenethyl-1*H*-pyrazole-4-carbonitrile, 3. Commercially available 2-(ethoxymethylene)malononitrile (**2**, 1.22 g, 10.0 mmol) was added portionwise to an ice-cooled solution of phenethylhydrazine (**1**, 1.36 g, 10.0 mmol) in ethanol. Once the addition was complete, the reaction mixture was refluxed under stirring until the disappearance of the starting materials (TLC

dx.doi.org/10.1021/jm401358b | J. Med. Chem. 2014, 57, 1225−1235

analysis). After the mixture was cooled to room temperature, the solid was collected by filtration and purified by crystallization from toluene. Mp 166−170 °C. Yield: 56%. ^{1}H NMR (δ, ppm): 7.53 (s, 1H, H_3), 7.27−7.18 (m, 5H, ArH), 6.56 (s, 2H, NH_2, exc), 4.08 (t, 2H, J = 8.06 Hz), 2.93 (t, 2H, J = 8.06 Hz).

Synthesis of 1-Phenethyl-1*H*-pyrazolo[3,4-*d*]pyrimidin-4(5*H*)-one, 4. 5-Amino-1-phenethyl-1*H*-pyrazole-4-carbonitrile, **4** (0.21 g, 1.00 mmol) was suspended in formic acid (0.5 mL) and heated overnight under stirring at T = 120 °C. The resulting mixture was poured into crushed ice, and the separated solid was collected by filtration and purified by crystallization from methanol. Mp 244−248 (dec). Yield: 78%. ^{1}H NMR (δ, ppm): 12.10 (s, 1H, NH, exc), 8.05 (s, 1H, H_3), 7.99 (s, 1H, H_6), 7.20−7.06 (m, 5H, ArH), 4.49 (t, 2H, J = 7.08 Hz), 3.12 (t, 2H, J = 7.08 Hz).

Synthesis of 4-Chloro-1-phenethyl-1*H*-pyrazolo[3,4-*d*]-pyrimidine, 5. Vielsmeier complex ($POCl_3$, 40.0 mmol, and DMF, 40.0 mmol) was added dropwise to an ice-cooled solution of 1-phenethyl-1*H*-pyrazolo[3,4-*d*]pyrimidin-4(5*H*)-one (**4**, 10.0 mmol) in anhydrous dichloromethane. Once addition was complete, the mixture was refluxed under stirring until the disappearance of the starting material (24 h, TLC analysis, 5/5 AcOEt/petroleum ether, 60−80 °C). The mixture was then ice-cooled, and the excess of $POCl_3$ was quenched with water. The crude was extracted with dichloromethane, dried over $MgSO_4$, and evaporated to dyness in vacuo to afford the target 4-chloro-1-phenethyl-1*H*-pyrazolo[3,4-*d*]pyrimidine, **5**, which was exploited in the following reaction without further purification.

Synthesis of *N*-(3-Nitrobenzyl)-1-phenethyl-1*H*-pyrazolo-[3,4-*d*]pyrimidin-4-amine, 6. 4-Chloro-1-phenethyl-1*H*-pyrazolo-[3,4-*d*]pyrimidine **5** (0.258 g, 1.0 mmol), 3-nitrobenzylamine hydrochloride (0.188 g, 1.0 mmol), and Et_3N (0.278 mL, 2.0 mmol) were suspended in toluene and irradiated with microwave at a temperature of 80 °C for 5 min. The cooled residue was poured into crushed ice and the solid separated was collected by filtration and purified by crystallization from toluene to obtain the desired derivative, **6**, as a yellow solid. Mp 113−114 °C. Yield: 61%. ^{1}H NMR (δ, ppm): 8.90 (t, 1H, NH, J = 5.86 Hz, exc), 8.20−8.09 (m, 4H), 7.80 (d, 1H, J = 7.30 Hz), 7.62 (t, 1H, J = 7.81 Hz), 7.24−7.10 (m, 5H), 4.84 (d, 2H, J = 5.86 Hz), 4.51 (t, 2H, J = 7.08 Hz), 3.13 (t, 2H, J = 7.08 Hz).

Synthesis of *N*-(3-Aminobenzyl)-1-phenethyl-1*H*-pyrazolo-[3,4-*d*]pyrimidin-4-amine, 7. A solution of *N*-(3-nitrobenzyl)-1-phenethyl-1*H*-pyrazolo[3,4-*d*]pyrimidin-4-amine, **6** (0.374 g, 1.00 mmol), in absolute ethanol was added by 10% palladium on carbon (0.10 mmol) and hydrogenated at atmospheric pressure and room temperature until the disappearance of the starting material (TLC analysis). After filtration of the catalyst, the solvent was evaporated to dryness to give the target derivative, **7**, as a white solid which was purified by crystallization from toluene. Mp 120−122 °C. Yield: 83%. ^{1}H NMR (δ, ppm): 8.63 (t, 1H, exc, J = 5.86 Hz), 8.18 (s, 1H), 8.13 (s, 1H), 7.20−7.14 (m, 5H), 6.93 (t, 1H, J = 7.32 Hz), 6.49−6.39 (m, 3H), 5.02 (bs, 2H, NH_2, exc), 4.56 (d, 2H, J = 5.86 Hz), 4.49 (t, 2H, J = 6.84 Hz), 3.13 (t, 2H, J = 6.10 Hz).

General Procedure for the Synthesis of *N*-(3-((1-Phenethyl-1*H*-pyrazolo[3,4-*d*]pyrimidin-4-ylamino)methyl)phenyl)-4-substituted-benzamide, 8a−g. *N*-(3-Aminobenzyl)-1-phenethyl-1*H*-pyrazolo[3,4-*d*]pyrimidin-4-amine **7** (0.344 g, 1.00 mmol) was suspended either in anhydrous toluene (to obtain derivatives **8a−d**) or in anhydrous xylene (to obtain derivatives **8e−g**), and to it were added the suitable benzoyl chloride (1.00 mmol), Et_3N (1.00 mmol), and DMAP (12 mg, 0.1 mmol). The resulting mixture was refluxed under stirring until the disappearance of the starting material (TLC analysis). The crude so obtained was evaporated to dryness, and water was added. The resulting compound, separated as a white solid, was collected by filtration, purified through flash chromatography (eluting system 5/5 AcOEt/petroleum ether, 60−80 °C), and crystallized from the suitable solveny (Supporting Information, Tables 1-SI and 2-SI).

General Procedure for the Synthesis of 1-(3-((1-Phenethyl-1*H*-pyrazolo[3,4-*d*]pyrimidin-4-ylamino)methyl)phenyl)-3-urea, 9a−g. A suspension of *N*-(3-aminobenzyl)-1-phenethyl-1*H*-pyrazolo[3,4-*d*]pyrimidin-4-amine **7** (0.344 g, 1.00 mmol) and the suitable isocyanate (1.00 mmol) in toluene was irradiated with microwave at a temperature of 90 °C for 5 min. The cooled residue was then poured into crushed ice, and the solid obtained was collected by filtration and purified through crystallization from the suitable solvent and characterized with physicochemical and spectroscopic data (Supporting Information, Tables 3-SI and 4-SI).

General Procedure for the Synthesis of *N*-(3-((1-Phenethyl-1*H*-pyrazolo[3,4-*d*]pyrimidin-4-ylamino)methyl)phenyl)-sulfonamide, 10a−g. A solution of *N*-(3-aminobenzyl)-1-phenethyl-1*H*-pyrazolo[3,4-*d*]pyrimidin-4-amine **7** (0.344 g, 1.00 mmol) and the suitable sulfonyl chloride (1.00 mmol) in DMF solution was used. Then pyridine, 1 mL, was added and the mixture was left under stirring at room temperature until the disappearance of the starting materials (TLC analysis: 8/2 AcOEt/petroleum ether, 60−80 °C). Once the reaction was complete, the crude was ice-cooled and 1 M HCl was added. The solution was extracted with AcOEt, dried over $MgSO_4$, evaporated to dryness, and triturated with diethyl ether. The resulting solid was collected by filtration and recrystallized from the suitable solvent. (Supporting Information, Tables 5-SI and 6-SI).

Biology. Materials and Methods. Human recombinant protein tyrosine kinases VEGFR2, RET and RET^{V804L}, and Omnia Tyr peptide 7 kit were from Invitrogen. All solvents were from Sigma-Aldrich.

Tyrosine Kinase Assays. Assays were performed in 96-well microtiter plates using the Omnia Tyr peptide 7 kit and following a previously reported protocol.[36,37] Tests were carried out at 30 °C in a reaction mixture containing 5 μL of tyrosine kinase reaction buffer, 5 μL of tyrosine kinase substrate, 5 μL of 1 mM ATP, 5 μL of 1 mM DTT, 25 μL of ultrapure water, and 5 μL of 3 mU/μL of the target kinase, in a total volume of 50 μL. All the above reagents, except the protein, were incubated at 30 °C for 5 min. Protein was then added to start the reaction, which was monitored with the fluorescence meter Victor3 PerkinElmer at 360 nm (excitation) and 485 nm (emission). Kinase activity was calculated from a linear least-squares fit of the data for fluorescence intensity versus time.

Enzymatic Inhibition. The inhibitory activity of the test compounds was assayed by adding 5 μL of the inhibitor solution to the reaction mixture described above. All the products were dissolved in 100% DMSO and diluted to the appropriate concentrations with tyrosine kinase reaction buffer, provided by the kit. Final concentration of DMSO in assay solutions never exceed 1% and proved to have no effects on protein activity. The inhibitory effect of the products was routinely estimated at 100 μM. Those compounds found to be active were then tested at additional concentrations between 100 μM and 10 nM. For a proper comparison, vandetanib was employed as the reference standard. The determination of the IC_{50} values was performed by linear regression analysis of the log dose response curve, which was generated using at least five concentrations of the inhibitor causing an inhibition between 20% and 80%, with two replicates at each concentration. The 95% confidence limits (95% CL) were calculated from t values for $n - 2$, where n is the total number of determinations (Tables 1 and 2).

Cell Cultures and Viability Assays. Reagents and Cell Lines. Test compounds were dissolved in a stock solution of 10 mM in 100% dimethylsulfoxide for in vitro studies. The DMSO concentration in control media was the one used to dilute the highest concentration of test compounds in the same experiment. Recombinant human epidermal growth factor (EGF) and basic fibroblast growth factor (bFGF) were from PeproTechEC Ltd. (London, U.K.). Cell culture media MCDB131 and F-12K, fetal bovine serum (FBS), L-glutamine, penicillin, streptomycin, and antibiotics were from Gibco (Gaithersburg, MD). Type A gelatin from porcine skin, supplements, and all other chemicals not listed in this section were obtained from Sigma Chemical Co. (St. Louis, MO). Plastics for cell culture were supplied by Sarsted (Verona, Italy). Human umbilical vein endothelial cells (HUVEC; Clonetics, San Diego, CA) were maintained in MCDB131 culture medium supplemented with 10% heat-inactivated FBS, L-glutamine 2 mM, heparin 10 units/mL, EGF 10 ng/mL, and bFGF 5 ng/mL and kept in a humidified atmosphere of 5% CO_2 at 37 °C. Human medullary thyroid cancer cell line (TT; ATCC, Manassas, VA, USA) was maintained in 10% FBS F-12K medium supplemented with L-glutamine 2 mM and kept in a humidified atmosphere of 5% CO_2 at 37 °C. Normal human fibroblast cell line (HNDF) was maintained in

10% FBS fibroblast basal medium supplemented with L-glutamine 2 mM and kept in a humidified atmosphere of 5% CO_2 at 37 °C.

Proliferation Assay. In vitro chemosensitivity was tested on HUVEC, TT, and HNDF cell lines. Cells were plated in sterile 24-well plastic plates (which were coated with 1% of gelatin in the case of endothelial cells) and treated for 72 h (using 3×10^4 cells/well of normal and cancer cells, in 1 mL of medium) with added test compounds (50, 10, 5, 1, and 0.1 μM) or with added vehicle (DMSO) alone. At the end of the experiment, cells were harvested with trypsin/EDTA, and viable cells were quantified using the automatic cell counter ADAM MC digital B (Twin Helix, Milano, Italy). The data are presented as the percentage of vehicle-treated cells. The concentration of drugs that decreased cell count by 50% (IC_{50}) compared with controls was calculated by nonlinear fitting of experimental data. All experiments were repeated, independently, three times with at least nine samples for each concentration (Table 3).

Cell-Based Phospho-RET Inhibition Assay. TT cells (5×10^4 cells/well) were seeded and maintained with 1% FBS medium. After 24 h, cells were treated continuously for 72 h with test compounds at a concentration corresponding to the experimental IC_{50} of cell proliferation. At the end of the experiment, the medium was removed and cells were rinsed with ice-cold PBS and directly lysed with 0.5 mL of ice-cold 1× lysis buffer (20 mM Tris, pH 7.5, 150 mM, 1 mM EDTA, 1 mM EGTA, 1% Triton X-100, 2.5 mM sodium pyrophosphate, 1 mM β-glycerol phosphate, 1 mM Na_3VO_4, 1 μg/mL leupetin; Cell Signaling Technology, MA, USA, catalog no. 9803) and 1 mM PMSF to each plate for 5 min at 4 °C. Lysates were collected and sonicated on ice for 10 s. The samples were microcentrifuged for 10 min at 4 °C, and the supernatant was collected. Cell lysates were assayed per manufacturer's instructions with PathScan1 phospo-ret (panTyr) and Total Ret sandwich ELISA kits (Cell Signaling Technology). The optical density was determined using the microplate reader Multiskan Spectrum (Thermo Labsystems, Milan, Italy) set to 450 nm. All experiments were repeated independently six times with at least nine samples for each concentration (Table 4).

Molecular Modeling. VEGFR-2 and RET X-ray Selection. So far, more than 30 X-ray structures are available in PDB for the VEGFR2 kinase. A detailed comparison of all these structures shows that, depending on the inhibitor type, the tyrosine kinase domain of VEGFR2 undergoes important conformational rearrangements: (i) at DFG activation loop level (DFG_{in} = loop in active conformation, inhibitor type I, and DFG_{out} = loop in inactive conformation, inhibitor type II); (ii) at the juxtamembrane level (JM_{in} = autoinhibitory conformation, inhibitor type IV; JM_{out} = nonautoinhibitory conformation, inhibitor type II).[33]

Thus, we initially selected for docking studies eight X-ray structures representative for the enzyme flexibility (Supporting Information, Table 8-SI), preferring those cocrystallized with ligands similar to our reference compound (**CLM3**, Chart 1). Particularly, we chose 1YWN as representative of the DFG_{in} conformation, while 2XIR, 3VHE, 4ASE, 4AGC, 4ASD, 4AGD, and 4AG8 have been chosen to represent the DFG_{out} and JM_{in}/JM_{out} conformations. Among these, the structure 4AG8 was used because it was demonstrated to be the best performing one in Glide cross-docking experiments. In particular, employing this structure, Glide was able to reproduce almost all the X-ray conformations of all the analyzed cocrystal ligands with an average root mean squared deviation (rmsd) of 3.33 Å (Supporting Information, Table 9-SI).

As for the RET X-ray selection, a detailed comparison among the phosphorylated structures currently available, superposing on the α carbon atoms using 2IVV[32] as the reference, indicated that the protein folding was highly preserved. A further analysis of two structures with the highest resolutions (2IVV and 2X2L[38]), both cocrystallized with an organic inhibitor, reveals that the K758 can assume different orientations upon ligand binding. In fact, in 2X2L, the phenylmethylidenedihydroindolone inhibitor does not occupy the N-lobe hydrophobic cavity, and the K758 partially blocks the pocket entrance. Conversely, the PP1 inhibitor in 2IVV enters the small cavity with its methylphenyl moiety forcing the long K758 side chain to shift its orientation. Cross-docking experiments showed that 2IVV can allocate also larger inhibitors like vandetenib, while 2X2L does not. Thus, 2IVV was chosen for our docking experiments.

Dockings. The binding mode of **CLM3** was studied by means of docking experiments, with the Glide tool available in the Maestro Package of Schrodinger, version 9.1.[39] The 3D structure of the ligand was generated with the Maestro fragment Build tool and then geometrically optimized with Macromodel. The VEGFR-2 and RET proteins structures were prepared through the Protein Preparation Wizard of the Maestro 9.1 graphical user interface which assigns bond orders, adds hydrogen atoms, deletes water molecules, and generates appropriate protonation states.[39]

The docking grid box was centered on the reference ligand for each X-ray structure, and docking runs were carried out using the standard precision (SP) method. The selected docking pose was minimized using OPLSA2005 as force field, the PRCG methods until a gradient of 0.001 kcal/(mol·Å^2) was obtained, and the implicit water model implemented in Macromodel.[40] Figures were rendered by the Chimera software package.[40]

■ ASSOCIATED CONTENT

Supporting Information

Tables 1-SI to 9-SI, including physical, spectral, computational, and purity data of compounds described, and Figure 1-SI, including putative binding poses of **8b** and **9c** in the active site of VEGFR-2. This material is available free of charge via the Internet at http://pubs.acs.org.

■ AUTHOR INFORMATION

Corresponding Author

*Phone: (+)39 050 2219593. Fax: (+)39 050 2219605. E-mail: concettina.lamotta@farm.unipi.it.

Notes

The authors declare no competing financial interest.

■ ACKNOWLEDGMENTS

The study has been funded in part by the Ministero dell'Istruzione, dell'Università e della Ricerca (MIUR), to C.L.M. and in part by the Associazione Italiana per la Ricerca sul Cancro (AIRC) to G.B.

■ ABBREVIATIONS USED

TC, thyroid carcinoma; MTC, medullary thyroid carcinoma; PTC, papillary thyroid carcinoma; DePTC, dedifferentiated thyroid carcinoma; EGFR, epidermal growth factor receptor; RET, REarranged during Transfection; VEGF, vascular endothelial growth factor; VEGFR2, vascular endothelial growth factor receptor 2; ATP, adenosine triphosphate; RDP, regulatory domain pocket

■ REFERENCES

(1) Ito, Y.; Nikiforov, Y. E.; Schlumberger, M.; Vigneri, R. Increasing incidence of thyroid cancer: controversies explored. *Nat. Rev. Endocrinol.* **2013**, *9*, 178−184.

(2) Aschebrook-Kilfoy, B.; Schechter, R. B.; Shih, Y. C.; Kaplan, E. L.; Chiu, B. C.; Angelos, P.; Grogan, R. H. The clinical and economic burden of a sustained increase in thyroid cancer incidence. *Cancer Epidemiol. Biomarkers Prev.* **2013**, *22*, 1252−1259.

(3) Boufraqech, M.; Patel, D.; Xiong, Y.; Kebebew, E. Diagnosis of thyroid cancer: state of art. *Expert Opin. Med. Diagn.* **2013**, *7*, 331−342.

(4) Vini, L.; Harmer, C. Management of thyroid cancer. *Lancet Oncol.* **2002**, *3*, 407−414.

(5) Stassi, G.; Todaro, M.; Zerilli, M.; Ricci-Vitiani, L.; Di Liberto, D.; Patti, M.; Florena, A.; Di Gaudio, F.; Di Gesù, G.; De Maria, M.

Thyroid cancer resistance to chemotherapeutic drugs via autocrine production of interleukin-4 and interleukin-10. *Cancer Res.* **2003**, *63*, 6784−6790.
(6) Ye, L.; Santarpia, L.; Gagel, R. F. The evolving field of tyrosine kinase inhibitors in the treatment of endocrine tumors. *Endocr. Rev.* **2010**, *31*, 578−599.
(7) Elisei, R.; Cosci, B.; Romei, C.; Bottici, V.; Ronzini, G.; Molinaro, E.; Agate, L.; Vivaldi, A.; Faviana, P.; Basolo, F.; Miccoli, P.; Berti, P.; Pacini, F.; Pinchera, A. Prognostic significance of somatic RET oncogene mutations in sporadic medullary thyroid cancer: a 10-year follow-up study. *J Clin. Endocrinol. Metab.* **2008**, *93*, 682−687.
(8) Lanzi, C.; Cassinelli, G.; Nicolini, V.; Zunino, F. Targeting RET for thyroid cancer therapy. *Biochem. Pharmacol.* **2009**, *77*, 297−309.
(9) Biglietto, G.; Maglione, D.; Rambaldi, M.; Cerutti, J.; Romano, A.; Trapasso, F.; Fedele, M.; Ippolito, P.; Chiappetta, G.; Botti, G. Upregulation of vascular endothelial growth factor (VEGF) and downregulation of placenta growth factor (PlGF) associated with malignancy in human thyroid tumors and cell lines. *Oncogene* **1995**, *11*, 1569−1579.
(10) Knauf, J. A. Does the epidermal growth factor receptor play a role in the progression of thyroid cancer? *Thyroid.* **2011**, *21*, 1171−1174.
(11) Ye, L.; Santarpia, L.; Gagel, R. F. Targeted therapy for endocrine cancer: the medullary thyroid carcinoma paradigm. *Endocr. Pract.* **2009**, *15*, 597−604.
(12) Gild, M. L.; Bullock, M.; Robinson, B. G.; Clifton-Bligh, R. Multikinase inhibitors: a new option for the treatment of thyroid cancer. *Nat. Rev. Endocrinol.* **2011**, *7*, 617−624.
(13) Wilhelm, S. M.; Adnane, L.; Newell, P.; Villanueva, A.; Llovet, J. M.; Lynch, M. Preclinical overview of sorafenib, a multikinase inhibitor that targets both Raf and VEGF and PDGF receptor tyrosine kinase signaling. *Mol. Cancer Ther.* **2008**, *7*, 3129−3140.
(14) Gan, H. K.; Seruga, B.; Knox, J. J. Sunitinib in solid tumors. *Expert Opin. Invest. Drugs* **2009**, *18*, 821−834.
(15) Mologni, L.; Redaelli, S.; Morandi, A.; Plaza-Menacho, I.; Gambacorti-Passerini, C. Ponatinib is a potent inhibitor of wild-type and drug-resistant gatekeeper mutant RET kinase. *Mol. Cell. Endocrinol.* **2013**, *377*, 1−6.
(16) Santos, E. S.; Gomez, J. E.; Raez, L. E. *Invest. New Drugs* **2012**, *30*, 1261−1269.
(17) Kelly, R. J.; Rixe, O. Axitinib—a selective inhibitor of the vascular endothelial growth factor (VEGF) receptor. *Target Oncol.* **2009**, *4*, 297−305.
(18) Bible, K. C.; Suman, V. J.; Menefee, M. E.; Smallridge, R. C.; Molina, J. R.; Maples, W. J.; Karlin, N. J.; Traynor, A. M.; Kumar, P.; Goh, B. C.; Lim, W. T.; Bossou, A. R.; Isham, C. R.; Webster, K. P.; Kukla, A. K.; Bieber, C.; Burton, J. K.; Harris, P.; Erlichman, C.; Mayo Phase 2 Consortium; Mayo Clinic Endocrine Malignances Disease Oriented Group.. A multiinstitutional phase 2 trial of pazopanib monotherapy in advanced anaplastic thyroid cancer. *J. Clin. Endocrinol. Metab.* **2012**, *97*, 3179−3184.
(19) Durante, C.; Paciaroni, A.; Plasmati, K.; Trulli, F.; Filetti, S. Vandetanib: opening a new treatment practice in advanced medullary thyroid carcinoma. *Endocrine* **2013**, *44*, 334−342.
(20) Nagilla, M.; Brown, R. L.; Cohen, E. E. Cabozantinib for the treatment of advanced medullary thyroid cancer. *Adv Ther.* **2012**, *29*, 925−934.
(21) Chaud, N. G.; Haddad, R. I. Vandetanib for the treatment of medullary thyroid cancer. *Clin. Cancer Res.* **2012**, *19*, 1−6.
(22) Lombardo, F.; Baudin, E.; Chiefari, E.; Arturi, F.; Bardet, S.; Caillou, B.; Conte, C.; Dallapiccola, B.; Giuffrida, D.; Bidart, J. M.; Schlumberger, M.; Filetti, S. Familial medullary thyroid carcinoma: clinical variability and low aggressiveness associated with RET mutation at codon 804. *J. Clin. Endocrinol. Metab.* **2002**, *87*, 1674−1680.
(23) Radi, M.; Tintori, C.; Musumeci, F.; Brullo, C.; Zamperini, C.; Drenassi, E.; Fallacara, A.; Vignaioli, G.; Crespan, E.; Zanoli, S.; Laurenzana, I.; Filippi, I.; Maga, G.; Schenone, S.; Angelucci, A.; Botta, M. Design, synthesis, and biological evaluation of pyrazolo[3,4-*d*]pyrimidines active in vivo on the Bcr-Abl T315I mutant. *J. Med. Chem.* **2013**, *56*, 5382−5394.
(24) Yang, L. L.; Li, G. B.; Ma, S.; Zou, C.; Zhou, S.; Sun, Q. Z.; Cheng, C.; Chen, X.; Wang, L. J.; Feng, S.; Li, L. L.; Yang, S. Y. Structure−activity relationship studies of pyrazolo[3,4-*d*]pyrimidine derivatives leading to the discovery of a novel multikinase inhibitor that potently inhibits FLT3 and VEGFR2 and evaluation of its activity against acute myeloid leukemia in vitro and in vivo. *J. Med. Chem.* **2013**, *56*, 1641−1655.
(25) Dinér, P.; Alao, J. P.; Söderlund, J.; Sunnerhagen, P.; Grøtli, M. Preparation of 3-substituted-1-isopropyl-1*H*-pyrazolo[3,4-*d*]pyrimidin-4-amines as RET kinase inhibitors. *J. Med. Chem.* **2012**, *55*, 4872−4876.
(26) Le Brazidec, J. Y.; Pasis, A.; Tam, B.; Boykin, C.; Black, C.; Wang, D.; Claassen, G.; Chong, J. H.; Chao, J.; Fan, J.; Nguyen, K.; Silvian, L.; Ling, L.; Zhang, L.; Choi, M.; Teng, M.; Pathan, N.; Zhao, S.; Li, T.; Taveras, A. Synthesis, SAR and biological evaluation of 1,6-disubstituted-1*H*-pyrazolo[3,4-*d*]pyrimidines as dual inhibitors of Aurora kinases and CDK1. *Bioorg. Med. Chem. Lett.* **2012**, *22*, 2070−2074.
(27) Antonelli, A.; Bocci, G.; La Motta, C.; Ferrari, S. M.; Fallahi, P.; Fioravanti, A.; Sartini, S.; Minuto, M.; Piaggi, S.; Corti, A.; Alì, G.; Berti, P.; Fontanini, G.; Danesi, R.; Da Settimo, F.; Miccoli, P. Novel pyrazolopyrimidine derivatives as tyrosine kinase inhibitors with antitumoral activity in vitro and in vivo in papillary dedifferentiated thyroid cancer. *J. Clin. Endocrinol. Metab.* **2011**, *96*, E288−E296.
(28) Bocci, G.; Fioravanti, A.; La Motta, C.; Orlandi, P.; Canu, B.; Di Desidero, T.; Mugnaini, L.; Sartini, S.; Cosconati, S.; Frati, R.; Antonelli, A.; Berti, P.; Miccoli, P.; Da Settimo, F.; Danesi, R. Antiproliferative and proapoptotic activity of CLM3, a novel multiple tyrosine kinase inhibitor, alone and in combination with SN-38 on endothelial and cancer cells. *Biochem. Pharmacol.* **2011**, *81*, 1309−1316.
(29) Zhang, J.; Yin, Z.; Leonard, P.; Wu, J.; Sioson, K.; Liu, C.; Lapo, R.; Zheng, S. A variation of the Fischer indolization involving condensation of quinone monoketals and aliphatic hydrazines. *Angew. Chem., Int. Ed.* **2013**, *52*, 1753−1757.
(30) *Glide*, version 5.5; Schrodinger, LLC: New York, 2009.
(31) McTigue, M.; Murray, B. W.; Chen, J. H.; Deng, Y. L.; Solowiej, J.; Kania, R. S. Molecular conformations, interactions, and properties associated with drug efficiency and clinical performance among VEGFR TK inhibitors. *Proc. Natl. Acad. Sci. U.S.A.* **2012**, *109*, 18281−18289.
(32) Knowles, P. P.; Murray-Rust, J.; Kjaer, S.; Scott, R. P.; Hanrahan, S.; Santoro, M.; Ibáñez, C. F.; McDonald, N. Q. Structure and chemical inhibition of the RET tyrosine kinase domain. *J. Biol. Chem.* **2006**, *281*, 33577−33587.
(33) McTigue, M.; Murray, B. W.; Chen, J. H.; Deng, Y.-L.; Solowiej, J.; Kania, R. S. Molecular conformations, interactions, and properties associated with drug efficiency and clinical performance among VEGFR TK inhibitors. *Proc. Natl. Acad. Sci. U.S.A.* **2012**, *109*, 18281−18289.
(34) Kubo, K.; Shimizu, T.; Ohyama, S.; Murooka, H.; Iwai, A.; Nakamura, K.; Hasegawa, K.; Kobayashi, Y.; Takahashi, N.; Takahashi, K.; Kato, S.; Izawa, T.; Isoe, T. Novel potent orally active selective VEGFR-2 tyrosine kinase inhibitors: synthesis, structure−activity relationships, and antitumor activities of *N*-phenyl-*N*′-{4-(4-quinolyloxy)phenyl}ureas. *J. Med. Chem.* **2005**, *48*, 1359−1366.
(35) Verbeek, H. H. G.; Alves, M. M.; de Groot, J.-V. B.; Osinga, J.; Plukker, J. T. M.; Links, T. P.; Hofstra, R. M. W. The effects of four different tyrosine kinase inhibitors on medullary and papillary thyroid cancer cells. *J. Clin. Endocrinol. Metab.* **2011**, *96*, E991−E995.
(36) Perspicace, E.; Jouan-Hureaux, V.; Ragno, R.; Ballante, F.; Sartini, S.; La Motta, C.; Da Settimo, F.; Chen, B.; Kirsch, G.; Schneider, S.; Faivre, B.; Hesse, S. Design, synthesis and biological evaluation of new classes of thieno[3,2-*d*]pyrimidinone and thieno-[1,2,3]triazine as inhibitor of vascular endothelial growth factor receptor-2 (VEGFR-2). *Eur. J. Med. Chem.* **2013**, *63*, 765−781.

(37) La Motta, C.; Sartini, S.; Tuccinardi, T.; Nerini, E.; Da Settimo, F.; Martinelli, A. Computational studies of epidermal growth factor receptor: docking reliability, three-dimensional quantitative structure−activity relationship analysis, and virtual screening studies. *J. Med. Chem.* **2007**, *52*, 964−975.
(38) Mologni, L.; Rostagno, R.; Brussolo, S.; Knowles, P. P.; Kjaer, S.; Murray-Rust, J.; Rosso, E.; Zambon, A.; Scapozza, L.; Mcdonald, N. Q.; Lucchini, V.; Gambacorti-Passerini, C. Synthesis, structure−activity relationship and crystallographic studies of 3-substituted indolin-2-one RET inhibitors. *Bioorg. Med. Chem.* **2010**, *18*, 1482−1496.
(39) *Maestro*, version 9.1; Schrödinger, LLC: New York, 2009; http://www.schrodinger.com/ (accessed May 15, 2011).
(40) Pettersen, E. F.; Goddard, T. D.; Huang, C. C.; Couch, G. S.; Greenblatt, D. M.; Meng, E. C.; Ferrin, T. E. UCSF chimera: a visualization system for exploratory research and analysis. *J. Comput. Chem.* **2004**, *25*, 1605−1612.